JPhys Energy

Developing a two-parabolic band model for thermoelectric transport modelling using Mg_2Sn as an example

Journal of Physics: Energy

OPEN ACCESS

RECEIVED
7 February 2022

REVISED
10 May 2022

ACCEPTED FOR PUBLICATION
8 July 2022

PUBLISHED
4 August 2022

PAPER

Developing a two-parabolic band model for thermoelectric transport modelling using Mg_2Sn as an example

H Naithani[1,*], **E Müller**[1,2] **and J de Boor**[1,3,*]

[1] Institute of Materials Research, German Aerospace Center (DLR), Cologne, Germany
[2] Institute of Inorganic and Analytical Chemistry, Justus Liebig University of Giessen, Giessen, Germany
[3] University of Duisburg–Essen, Institute of Technology for Nanostructures (NST), D–47057 Duisburg, Germany
[*] Authors to whom any correspondence should be addressed.

E-mail: Harshita.Naithani@dlr.de **and** johannes.deboor@dlr.de

Keywords: thermoelectrics, electronic band structure, SPB model, multiband model, minority carrier effects, carrier concentration optimization, band gap

Supplementary material for this article is available online

Abstract

Thermoelectrics is a field driven by material research aimed at increasing the thermal to electrical conversion efficiency of thermoelectric (TE) materials. Material optimisation is necessary to achieve a high figure of merit (zT) and in turn a high conversion efficiency. Experimental efforts are guided by the theoretical predictions of the optimum carrier concentration for which generally the single parabolic band (SPB) model is used which considers the contribution to electronic transport only from the majority carriers' band. However, most TE materials reach peak performance (maximum zT) close to their maximum application temperature and when minority carrier effects become relevant. Therefore, single band modelling is insufficient to model the behaviour of TE materials in their most practically relevant temperature range. Inclusion of minority effects requires addition of the minority carrier band and necessitates the use of a two-band model—the simplest and, for most cases, sufficient improvement. In this study, we present a systematic methodology for developing a two-band model using one valence and one conduction band for any given TE material. The method utilises in part the SPB model and in part a simple cost function based analysis to extract material parameters like density of states masses, band gap, deformation potential constant etc., based on easily available experimental data. This simple and powerful method is exemplified using Mg_2Sn, chosen due to its low band gap, the availability of experimental data in a wide range of dopant concentrations and its practical importance, being an end member of the highly popular $Mg_2(Si,Sn)$ solid solutions. Using the experimental data for p- and n-type Mg_2Sn from literature, a two-band model was obtained. Optimum carrier concentration and maximum zT were predicted from both SPB and two-band models and at 650 K pronounced differences between the two models, which could prevent realisation of maximum zT, were observed, demonstrating the practical necessity to model the effect of minority carriers.

1. Introduction

Thermoelectric (TE) materials utilize temperature differences to generate electricity and vice versa [1–3]. They have a promising application in the conversion of waste heat into electricity, thereby acting as generators [4, 5]. However, their application is limited by their low efficiency. Usually the goodness of a TE material is determined by a figure of merit (zT) whose higher value corresponds to higher efficiency. Thus, there is a drive among researchers to increase zT [6] by finding new materials [7, 8] or by modifying existing materials via band structure or defect engineering [9–14], carrier concentration optimization [15], etc. The TE figure of merit zT is a function of the carrier concentration, and peaks in the range of 10^{18}–10^{20} cm^{-3} for most materials, the exact value depending on material and temperature. Therefore, n, in a given material, is usually tuned to get the highest possible zT at a given temperature. Purely experimental optimization within

such a wide range would be tedious. This makes modelling of TE materials essential. While TE materials' properites can be modelled from first principles using density functional theory (DFT), accurate DFT-based calculations are somewhat involved. On the other hand, the simpler single parabolic band (SPB) model, which assumes that only one band participates in the charge transport, is employed readily based on analytical formulae and without dedicated software [16–21]. This assumption can be justified in materials with relatively large band gaps (with respect to the targeted operational temperature range). Furthermore, there should also be a large inter-band separation between the first and the second majority carrier band. SPB modeling has been employed successfully in many material systems like $Mg_2(Si,Sn)$ [22], ZnSb [17], Bi_2Te_3 [23], PbTe [24, 25], etc. even though a single band model cannot describe all transport details realistically. A single band is, of course, not enough to capture the complete picture of the material when more than one majority carrier band [26–28] and/or minority carrier bands are contributing substantially to charge transport. Particularly, the minority carrier density scales roughly with $\exp\left(-E_g/2k_BT\right)$ and the band gap itself decreases with increasing temperature for most materials [29, 30]. Its effect is clearly visible in the experimental transport data at high temperatures for many materials. Based on this, in heavily doped (HD) materials, temperature dependent TE properties' data can be divided into two parts—a low temperature range where only majority carriers are relevant (the extrinsic range) and a high temperature range where minority carriers are also relevant (bipolar conduction, usually close to and above the region of maximum zT).

The main target of optimization is to ultimately have TE devices operating at maximum efficiency. Therefore, without a correct optimum carrier concentration prediction for the material to be used in a device, material optimization remains empirical and tedious and the potential of the material might not be exploited fully. Inclusion of minority carrier effects can be achieved using a two parabolic band (2PB) model with one valence band (VB) and one conduction band (CB). It could be argued, if accurate optimization is needed, then why stop at two bands and not include more bands? In principle this can be done and will give an even more accurate picture of the material, but with substantially increased complexity due to more unknown parameters to be considered. However, the increase in accuracy will be minor if the second lowest conduction and the second highest VBs are far enough from the lowest conduction and highest VBs, respectively, to be of any practical consequence. In such cases, working with a two-band model is not only the easiest improvement to the SPB model but would also be sufficiently accurate for predicting zT vs n for most materials. Interestingly, applications of such band structure modelling also go beyond standard thermoelectric materials; for example, Chasapis *et al* use a two-band model to interpret the transition from p- to n-type in ternary tetradymite topological insulators [31].

Here we present a method which, like SPB modelling, extracts band structure-related parameters from the experimental data itself. This is in contrast to obtaining material parameters from DFT—which is a purely theoretical approach. DFT calculations are usually done at 0 K while material parameters are required at higher temperatures. Thus, in many cases there are discrepancies between the experimental and DFT results for material parameters [32, 33]. Moreover, within DFT, different calculation methods, particularly the choice of different functionals, lead to different results for the same material [33, 34]. The band gap—a crucial material parameter for modelling TE properties is often strongly underestimated in DFT calculations [35, 36]. Furthermore, while DFT methods can be employed with considerable success to predict band structures, calculation of correct scattering rates for charge carriers remains a considerable challenge; often the constant relaxation time approximation is employed [37–40]. Therefore, when relatively simple, obtaining material parameters from experimental data is advantageous because one can get 'effective' values, sufficient for material optimization.

The method described in this paper is systematic and utilizes an SPB model and a cost function-based analysis to find material parameters. It requires availability of the experimental data for both p- and n-type materials which could be either taken from literature or obtained by synthesizing samples with the desired compositions. To illustrate this method, Mg_2Sn was chosen as an example due to the following reasons. Generally, members of Mg_2X (with X = Si, Ge, Sn) and their solid solutions are a very promising class of materials [41, 42] with $Mg_2Si_{1-x}Sn_x$ solid solutions most attractive for industrial applications. They have two relevant CBs and (at least) one relevant VBs with a convergence of the CBs at around $x = 0.6, 0.7$ [22], thus demanding at least a three-band model to describe the n-type properties adequately. However, developing a three-band model is much more difficult due to many unknown parameters, a problem generally tackled by making simplifying assumptions which may not necessarily be accurate. For example, a three-band model for $Mg_2Si_{0.4}Sn_{0.6}$ has been developed by Zhang *et al* [43] with the large parameter space reduced by taking some parameters values from literature and assuming some parameter values to be same for the three bands considered. A further complication of the solid solutions is that they can de-mix into Mg_2Si- and Mg_2Sn-rich regions [44–47], potentially requiring the use of effective medium models for accurate descriptions. Among Mg_2Si and Mg_2Sn, the latter has a lower band gap, with values varying between 0.1 and 0.3 eV [33, 48–51].

On the other side, for Mg_2Si the reported band gap is between 0.6–0.7 eV [51]. Therefore, minority carrier effects are more strongly visible in Mg_2Sn, even at mid-range temperatures and high carrier concentrations. With respect to the second CB, the reported inter-band separation between the two CBs from *ab-initio* calculations for Mg_2Sn ranges from 0.16 to 0.4 eV at 0 K [51], justifying neglecting the upper band at least as a starting point. Additionally, TE property data for Mg_2Sn is available for both p- and n-type materials [52, 53] in a wide range of carrier concentrations and temperatures. Finally, it should be pointed out that a 2PB modelling of Mg_2Sn is not merely a theoretical exercise, because studying end members can lead to insights helpful for their more practically interesting solid solutions. Moreover, Mg_2Sn has sparked some interest as a potential TE material in its own right due to its relatively high power factor for both n- and p-type material [40, 52–54].

2. Methodology

The method of obtaining material parameters presented here is a combination of SPB modelling and mathematical optimization. The first part of the method—SPB modelling, is applicable when one effective band is sufficient to describe material transport. It is successful in HD materials with only one majority carrier band or several degenerate (or almost degenerate) bands so that they can still be modelled by one effective band [22]. The second part of the method—mathematical optimization, is used to obtain the best fit for TE properties by optimizing the value of a particular modelling parameter. The optimization method employed here is the least square error method which is a simple cost function of the form [55]:

$$R = \sum_j \sum_i \left(1 - A^{(i)}_{j,\mathrm{exp}} / A^{(i)}_{j,\mathrm{mod}}\right)^2. \tag{1}$$

Here, the subscript 'exp' indicates the experimental value, 'mod' indicates the value obtained from the model, j is the index for the TE property and i is the index for the associated data point and R indicates the total relative error. A_j can be any measured TE property—Seebeck coefficient (S), electrical conductivity (σ), thermal conductivity (κ) or Hall coefficient (R_H). The choice of A_j depends on the availability of experimental data and its suitability for the intended optimization, as discussed ahead.

Since this method derives material parameters from experimental data, the first step is to collect experimental data. Temperature dependent TE data, i.e. S, σ, κ and R_H, for both p- and n-type materials are required. If a temperature dependent Hall measurement is difficult to accomplish, at least the room temperature Hall coefficient for the highly and moderately doped samples should be known. The terms of high, moderate and low doping are used here in a qualitative sense. A highly doped sample is one which largely follows an SPB model over the entire temperature range, a moderately doped sample follows SPB behavior in the low temperature range but shows minority carrier effects at high temperatures while a low doped sample does not have to necessarily follow SPB behavior in any temperature range. Highly doped materials' data are required to extract parameters like the DOS masses and mobility parameters using SPB. By means of moderately doped samples, extraction of the band gap can be attempted. Using the obtained parameters, the model can be tested on the entire dataset to check its applicability by including the low doped samples.

The stepwise procedure for using this method is given below. An excellent review of SPB modelling is given by May and Snyder [16] and therefore, is not explained in detail here. The equations are presented with the assumption of acoustic phonon scattering of the carriers [56] being the dominant scattering mechanism at and above room temperature. The stepwise procedure is:

(a) Highly doped samples' data are taken. Since the SPB model is applicable here, the carrier concentration, n, obtained from the room temperature Hall coefficient $\left(n = r_\mathrm{H}/eR_\mathrm{H} \text{ where } r_\mathrm{H} = \frac{3}{4}\left(\frac{F_{1/2}F_{-1/2}}{F_0^2}\right)\right)$, can be assumed to be equal to the carrier concentration at higher temperatures. Using the SPB equations, the DOS mass is calculated by obtaining the reduced Fermi level, η from the Seebeck coefficient and the DOS mass, m^*_D from the carrier concentration and Fermi level:

$$S = \left(\frac{k_\mathrm{B}}{e}\right)\left(\frac{2F_1(\eta)}{F_0(\eta)} - \eta\right) \tag{2}$$

$$n = 4\pi\left(\frac{2m^*_\mathrm{D}k_\mathrm{B}T}{h^2}\right)^{3/2} F_{\frac{1}{2}}(\eta). \tag{3}$$

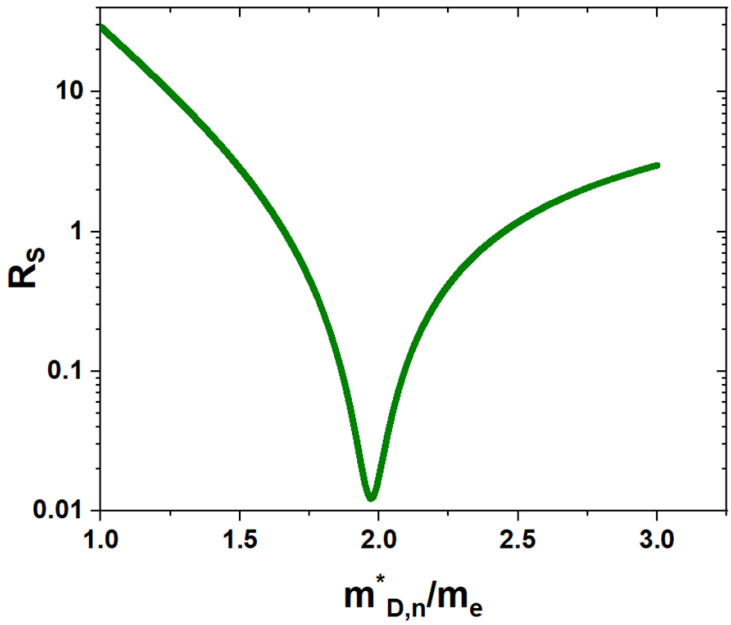

Figure 1. Illustration of the usage of a cost function for determining the best fit value of a parameter (here, the DOS mass in the conduction band ($m^*_{D,n}$) using equation (4)). m_e is the electron rest mass. $m^*_{D,n}$ has been found here using the Seebeck coefficient and room temperature Hall coefficient data for two heavily doped samples—$Sc_{0.05}Mg_{1.95}Sn_{0.97}Sb_{0.03}$ and $Mg_2Sn_{0.97}Sb_{0.03}$.

Here, k_B, e and h are the Boltzmann constant, elementary charge and Planck's constant, respectively, T is the temperature and F_j is the Fermi integral: $F_j(\eta) = \int_0^\infty \frac{\varepsilon^j d\varepsilon}{1+\exp(\varepsilon-\eta)}$. These equations are to be used for each (S,T) data point individually. If data are available for multiple samples, then m^*_D values are obtained for all data points and a single averaged mass can be taken which provides the best fit for the data. For averaging, the following cost function is used:

$$R_S = \sum_i \left(1 - S^{(i)}_{exp}/S^{(i)}_{mod}(m^*_D)\right)^2. \tag{4}$$

S_{mod} values are obtained using equations (3) and (2) (in that order) using variable m^*_D values to minimize equation (4). This step will give the DOS effective mass for the VB, $m^*_{D,p}$ and for the CB, $m^*_{D,n}$. This is illustrated in figure 1.

(b) Once m^*_D is known, the mobility parameter is obtained. The relationship between conductivity and mobility parameter, μ_0 is [16]:

$$\sigma = ne\mu_0 \frac{2}{3}\frac{F_0}{F_{1/2}}. \tag{5}$$

The mobility parameter due to acoustic phonon scattering is given by:

$$\mu_{0,AP} = \frac{\pi\sqrt{8}\hbar^4 e\rho {v_l}^2}{4E^2_{def}\, {m_s}^{2.5}(k_B T)^{3/2}}. \tag{6}$$

Here, ρ is the material density, v_l is the longitudinal velocity of sound, m_s is the single valley effective mass, $\hbar$ is the reduced Planck's constant and E_{def} is the deformation potential constant. If acoustic phonon scattering is the sole scattering mechanism to be considered, then E_{def} is the only unknown since other material parameters namely, ρ and v_l can be taken from literature. The valley degeneracy, N_v, needed to calculate $m_s = m^*_D/{N_v}^{2/3}$, is known from the band structure of the material. Thus, in a similar way as for the DOS mass, E_{def} (or μ_0) is obtained by minimizing the cost function:

$$R_\sigma = \sum_i \left(1 - \sigma^{(i)}_{exp}/\sigma^{(i)}_{mod}(E_{def})\right)^2. \tag{7}$$

For alloyed materials (like $Mg_2(Si,Sn)$ solid solutions), alloy scattering is also an important scattering mechanism [57] and can be included using Matthiessen's rule [53, 58]. However, in that case the alloy scattering potential constant will be an additional unknown parameter and would need to be evaluated.

Once the DOS masses and mobility parameters for the valence and CBs are extracted from the highly doped samples, the next step is to find the band gap. Now a two-band model needs to be considered.

(c) Thermal excitation of carriers is the phenomenon that takes a material from a single band to a 1 VB + 1 CB behavior. In an SPB model, the charge carrier concentration remains constant with temperature and originates from ionized dopant atoms or charged intrinsic defects. In the two-band model considered here, charge carriers are not only generated from charged defects but also when electrons in the VB gain sufficient thermal energy to overcome the band gap. Therefore, the total carrier concentration is now a function of temperature and can no longer be assumed to be equal to the dopant concentration. Charge neutrality equation is invoked here:

$$n_{\mathrm{A}}^{*} + n = n_{\mathrm{D}}^{*} + p. \tag{8}$$

Here, n_{A}^{*} and n_{D}^{*} denote the charge carrier concentrations due to the acceptors and donors, respectively, n is the total electron concentration and p denotes the total hole concentration. While the intrinsic carrier concentrations depend upon band gap and temperature, the extrinsic carrier concentration remains constant since practically all dopant atoms get ionized well below room temperature. If a sample shows SPB behavior in the low temperature range, then practically all carriers at room temperature are contributed by the dopant and the Hall carrier concentration at room temperature gives the dopant carrier concentration. If the same sample shows intrinsic behavior at high temperatures, it provides an opportunity to estimate the band gap since the magnitude of the band gap is the only remaining unknown. Therefore, at this stage, 'moderately doped' samples are used. The two-band equations to be used [16] are listed below. A rearranged charge neutrality equation is used with the net extrinsic carrier concentration, $N_{\mathrm{extrinsic}}$, expressed as the difference between the concentrations of the two types of carriers:

$$N_{\mathrm{extrinsic}} = n_{\mathrm{maj}} - n_{\mathrm{min}}. \tag{9}$$

Here, $N_{\mathrm{extrinsic}}$ is known from the room temperature Hall measurement. $n_{\mathrm{maj/min}}$ is replaced by the equation for charge carriers in a single band (equation (3)). It should be noted that the position of the reduced Fermi level is taken relative to that band's edge for which the transport property is being calculated. If the CB edge is taken as a reference, then the Fermi level with respect to the VB is given by:

$$\eta = -\psi - \varepsilon_G. \tag{10}$$

Here η and ψ are the reduced Fermi level relative to the valence and CBs, respectively and ε_G is the reduced band gap $\left(= E_{\mathrm{g}}/k_B T\right)$. Thus, the band gap, though not explicitly visible, is present in the two-band equations. Similarly, the equations for the other properties are:

$$S = \frac{S_{\mathrm{p}}\sigma_{\mathrm{p}} + S_{\mathrm{n}}\sigma_{\mathrm{n}}}{\sigma} \tag{11}$$

$$\sigma = \sigma_{\mathrm{p}} + \sigma_{\mathrm{n}} \tag{12}$$

$$R_{\mathrm{H}} = \frac{R_{\mathrm{H,n}}\sigma_n^2 + R_{\mathrm{H,p}}\sigma_p^2}{\sigma^2} \tag{13}$$

$$\kappa_{\mathrm{e}} = \kappa_{\mathrm{e,p}} + \kappa_{\mathrm{e,n}} + \kappa_{\mathrm{bip}} \tag{14}$$

$$\kappa_{\mathrm{bip}} = \frac{\sigma_{\mathrm{p}}\sigma_{\mathrm{n}}}{\sigma}\left(S_{\mathrm{p}} - S_{\mathrm{n}}\right)^2 T. \tag{15}$$

$\kappa_{\mathrm{e,n}}$ and κ_{bip} denote the (single carrier) electronic and bipolar thermal conductivity. Data for the heavily and the moderately doped samples are taken together, and the band gap is estimated using the following cost function given by equation (1). In principle, temperature dependent data for the Hall coefficient and thermal conductivity can be used. However, Hall data is usually more difficult to obtain and including thermal conductivity would require the *a priori* knowledge of lattice thermal conductivity, κ_{L} with $\kappa_{\mathrm{e}} = \kappa - \kappa_{\mathrm{L}}$, which is not easily accessible either. Therefore, using the Seebeck and electrical conductivity data, the cost function is given by:

$$R_{S+\sigma} = \sum_i \left(1 - S_{\mathrm{exp}}^{(i)}/S_{\mathrm{mod}}^{(i)}\right)^2 + \sum_i \left(1 - \sigma_{\mathrm{exp}}^{(i)}/\sigma_{\mathrm{mod}}^{(i)}\right)^2. \tag{16}$$

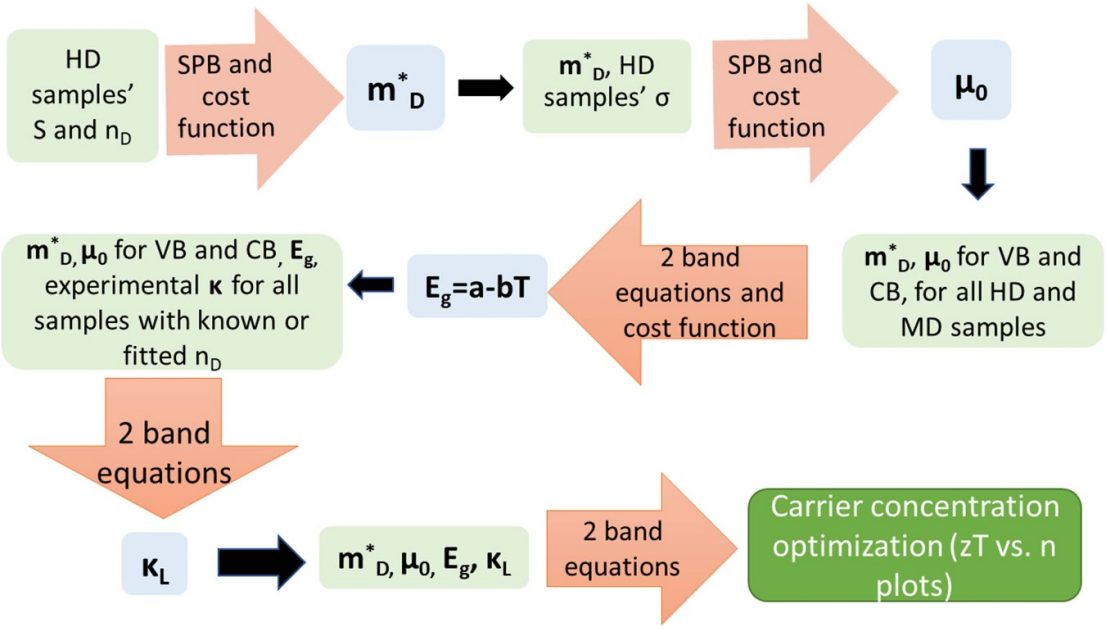

Figure 2. Schematic for determination of modelling parameters and the implementation of the two-band model. HD and MD are the abbreviations for heavily doped and moderately doped. Light green and light blue colored boxes contain the inputs and outputs, respectively.

If a linear temperature dependence of the form $E_g = E_{g,0} - bT$ is assumed for the band gap [50], then E_{g0} and b would have to be determined.

(d) Once these parameters are known, the two-band model can be applied to low doped samples as well to check for agreement. For low doped samples, dopant carrier concentrations are not directly available from room temperature Hall measurements since intrinsic carriers are not negligible. Therefore, dopant concentrations have to be estimated from fitting the dopant concentration to the TE data using the obtained two-band model. Getting a good match between the modelled and experimental data can validate the two-band model's parameters. An additional check would be to calculate lattice thermal conductivity, κ_L values. In equation (14), the electronic thermal conductivity is not only the sum of individual electronic thermal conductivities but also contains a quantitatively very significant additional term—bipolar thermal conductivity. If a material with a low band gap is analyzed with the SPB model, the calculated κ_L $(= \kappa - \kappa_e)$ will increase with temperature at higher temperatures, since the bipolar conductivity term is missing in the SPB model. As lattice thermal conductivity at room temperature and above is expected to decrease with temperature [59], this would indicate failure of SPB modelling. A two-band model, if accurate, should give κ_L which monotonously decreases with temperature.

(e) Once κ_L is obtained from the model (or is known from literature), zT vs n can be deduced to optimize the material. Alternately, power factor, PF vs n plots can also be generated if optimizing the power factor is the goal. A concise schematic of all the steps is shown in figure 2.

3. Results

Data for four Li-doped p-type [53] and four Sc- and/or Sb-doped n-type Mg_2Sn [52] samples were taken from literature. Among the p-type samples, $Li_{0.03}Mg_{1.97}Sn$ and $Li_{0.02}Mg_{1.98}Sn$ were identified as HD and $Li_{0.01}Mg_{1.99}Sn$ and $Li_{0.005}Mg_{1.995}Sn$ were identified as moderately doped. Among the n-type samples, $Sc_{0.05}Mg_{2.01}Sn_{0.97}Sb_{0.03}$ and $Mg_{2.06}Sn_{0.97}Sb_{0.03}$ were identified as HD and $Sc_{0.05}Mg_{1.95}Sn$ and $Sc_{0.01}Mg_{1.99}Sn$ were identified as low doped. n-type samples chosen for this work were nominally Sc-doped. However, Sc was found to be ineffective as a dopant and basically without effect on the electronic properties as it forms secondary phases (ScSn and ScSi) in the Mg_2Sn matrix, presumably without dissolving into $Mg_2(Si,Sn)$ [52]. While the effect of ScSn or ScSi phases cannot be excluded, the effect is expected to be small as they form distinct islands and have a small volume percentage and therefore should not be of great consequence while attempting two-band modelling. Additionally, data for an undoped Mg_2Sn sample [52] was available which showed p-type behavior in a large part of the temperature range and is displayed together with the Li-doped samples' data.

Table 1. Material parameters used in the two-band modelling. m_e is the electron rest mass.

Property	Valence band	Conduction band
DOS mass (m^*/m_e)	1.1	2
Deformation potential constant (eV)	9.5	6.7
Band gap (eV)	$0.28–2 \times 10^{-4}$ T/K	

Table 2. Samples with their extrinsic carrier concentrations.

p-type composition	Extrinsic carrier concentration (10^{20} cm^{-3})	n-type composition	Extrinsic carrier concentration (10^{20} cm^{-3})
$Li_{0.03}Mg_{1.97}Sn$	2.69	$Sc_{0.05}Mg_{2.01}Sn_{0.97}Sb_{0.03}$	4.57
$Li_{0.02}Mg_{1.98}Sn$	2.45	$Mg_{2.06}Sn_{0.97}Sb_{0.03}$	3.97
$Li_{0.01}Mg_{1.99}Sn$	1.51	$Sc_{0.05}Mg_{1.95}Sn$	2.00×10^{-2} (fitted)
$Li_{0.005}Mg_{1.995}Sn$	7.20×10^{-1} (fitted)	$Sc_{0.01}Mg_{1.99}Sn$	4.00×10^{-3} (fitted)
Mg_2Sn	4.40×10^{-2}		

Based on the methodology given above, p-type HD samples $Li_{0.03}Mg_{1.97}Sn$ and $Li_{0.02}Mg_{1.98}Sn$ and n-type HD samples, $Sc_{0.05}Mg_{2.01}Sn_{0.97}Sb_{0.03}$ and $Mg_{2.06}Sn_{0.97}Sb_{0.03}$ were used to determine the DOS masses and deformation potential constants for the VB and CB respectively. $\rho = 3590$ kg m^{-3}, $v_l = 4800$ m s^{-1} and $N_v = 3$ for the CB and $N_v = 2$ for VB were used in equation (6) [50, 53]. The band gap, assumed to depend on temperature by the law, $E_g = E_{g,0} - bT$ was determined next. For this, the cost function given by equation (16) was minimized to find the best $E_{g,0}$ value by fixing b at 1×10^{-4}, 2×10^{-4} and 3×10^{-4} K^{-1} making this a single parameter optimization process. Two-band modelling fits for these three sets of $E_{g,0}$ and b values were then compared to choose the best band gap parameters. Material parameters extracted from experimental data are given in table 1. The extrinsic carrier concentration for low doped samples could not be ascertained from the measured Hall coefficient since these samples showed two-band behavior from room temperature. Therefore, for the low doped samples, using equation (16) with the two-band model and the now known band structure parameters, extrinsic carrier concentrations were obtained by fitting. Extrinsic carrier concentrations for all samples are given in table 2.

Figure 3 shows the comparison between experimental and modeled Seebeck and electrical conductivities for all p- and n-type samples. For the Seebeck coefficient values, the theoretical fitting agrees well for all HD and moderately doped samples. The SPB model fits for two HD samples—$Li_{0.03}Mg_{1.97}Sn$ and $Sc_{0.05}Mg_{2.01}Sn_{0.97}Sb_{0.03}$—have also been shown and they are in good agreement with the 2PB model fits. For low doped n-type samples and the undoped sample, there is a mismatch between theoretical and experimental values.

4. Discussion

As seen in figures 3(b) and (d), there is a good agreement between the experimental and theoretical electrical conductivities for all samples. However, in figure 3(b), an exact match between theoretical and experimental electrical conductivity for the HD n-type samples is missing. This could be due to grain boundary scattering having an impact at low temperatures. This has been observed for Mg_2Si [60] and $Mg_2(Si,Sn)$ [61, 62] as well as for other material classes [63, 64]. The extent of grain boundary scattering apparently depends sensitively on the synthesis route and the synthesis parameters. It can therefore be included only on a sample to sample (or batch to batch) level, but not in a general manner. Furthermore, for Mg_2Sn and $Mg_2(Si,Sn)$ it is mainly observed at low T, where zT is small. With respect to material optimization it is therefore not crucial to include grain boundary scattering for the material system studied; this might be different for other material systems [64]. In the present case, there is a possibility of an additional relationship between Sc doping and a grain boundary influence. A fit for the HD sample $Sc_{0.05}Mg_{2.01}Sn_{0.97}Sb_{0.03}$ using the SPB model including grain boundary scattering [65] is shown in figure S1 in the supplementary info.

The methodology presented in this paper is advantageous due to its simplicity and it provided good fits for most of the data. The band gap, being a key parameter found using this methodology, was additionally estimated using the Goldsmid–Sharp method [66], even though it is known to have quite large uncertainties for the parameters of typical TE materials [67]. The Goldsmid–Sharp band gap estimate is given by $E_g = 2|S|_{max}T_{max}$. To use this equation, temperature dependent Seebeck data are needed for those samples whose absolute Seebeck attains a maximum. This was the case for all Li-doped samples and they were used to estimate the Goldsmid–Sharp band gap. Band gap values from fitting the Seebeck and electrical conductivity data and the Goldsmid–Sharp method are given in table 3 for comparison. There is a good agreement

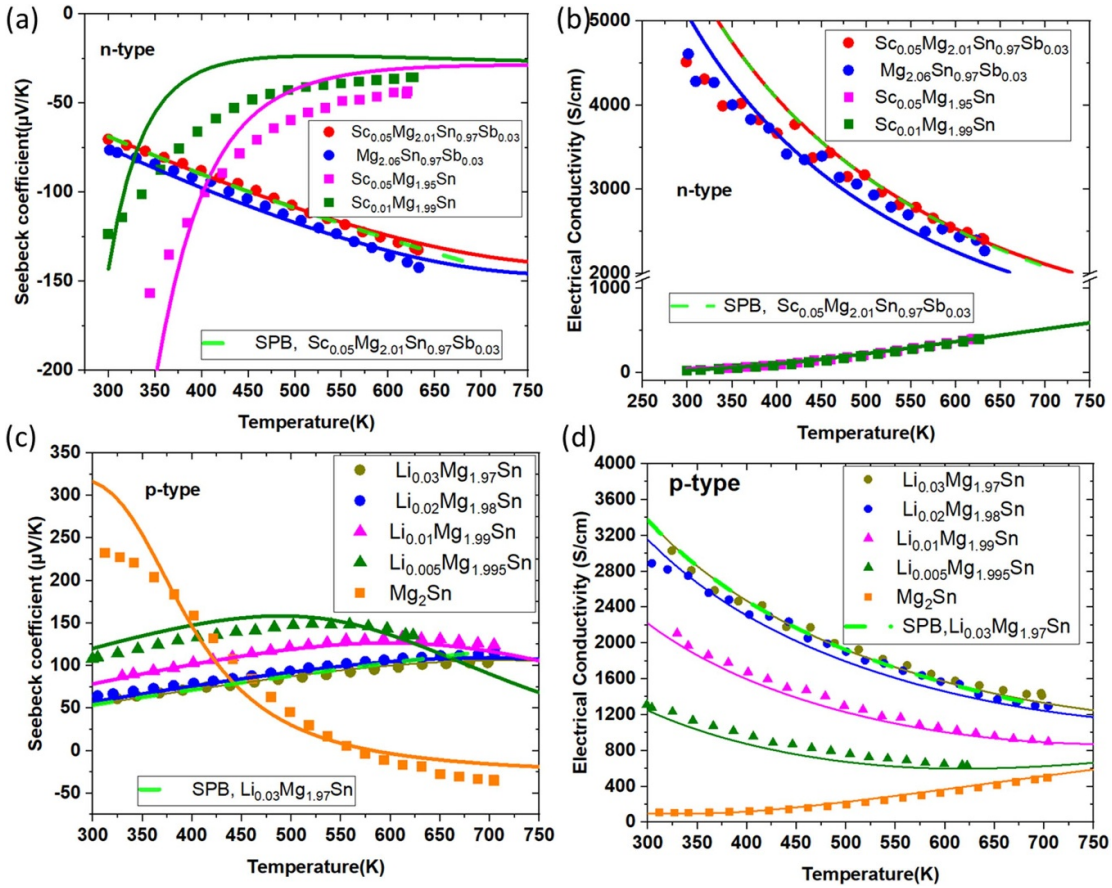

Figure 3. Seebeck coefficient (a) and (c) and electrical conductivity (b) and (d) for n-type and p-type Mg_2Sn. Points represent experimental data and solid lines represent theoretical fits from the two-band model. Circular, triangle and square symbols represent experimental data for heavily doped, moderately doped samples and lowly doped samples, respectively. Dashed lines represent SPB fitting with the same extrinsic carrier concentration as their two-band model counterparts.

Table 3. Band gap values estimated from the Seebeck and sigma data and the Goldsmid–Sharp method.

Sample composition	$T(S_{max})$ (K)	Goldsmid–Sharp gap (eV)	This work: $E_g = 0.28\text{–}2 \times 10^{-4}\ T\ K^{-1}$ eV
$Li_{0.03}Mg_{1.97}Sn$	761	0.16	0.13
$Li_{0.02}Mg_{1.98}Sn$	736	0.17	0.13
$Li_{0.01}Mg_{1.99}Sn$	620	0.17	0.17
$Li_{0.005}Mg_{1.995}Sn$	530	0.16	0.16

between the two methods. Also, our result for the room temperature value for the band gap is 0.22 eV which is within the reported range of band gap for Mg_2Sn of 0.1–0.3 eV [33, 48–51, 68].

The biggest advantage of the methodology described here is the reduced reliance on literature inputs for modelling parameters due to first, the relative simplicity of the two-band model and second, employing data for both p- and n-type material in a wide range of carrier concentration. Zhang *et al* [43] also used a stepwise method to develop a three-band (2 CB + 1 VB) model for $Mg_2Si_{0.4}Sn_{0.6}$. Only HD n-type data are used to develop the model, where holes are relevant only as minority carriers and the mass for the VB is taken from literature. To reduce the significantly higher number of unknowns, they assumed that all three bands have the same values for the scattering potential constants for alloy scattering and acoustic phonon scattering, which might not be accurate as can be seen from our results obtained independently for the valence and the CB as well as literature reports on other materials [69, 70]. At last, since we include (and recommend the inclusion of) low doped samples in our analysis, we have the opportunity to test the accuracy of the developed model as already seen in figure 3. An interesting and baffling feature of figure 3 is that while a good fit for the electrical conductivity is achieved with the two-band model for all samples, it is not as good for the Seebeck coefficient of the low doped samples. As mentioned earlier, different values for the temperature parameter b were fixed first and then the parameter $E_{g,0}$ was optimized. It was observed that a better fit for Seebeck was achieved with lower values of b with best fit for Seebeck achieved at $E_{g,0} = 0.16$ eV

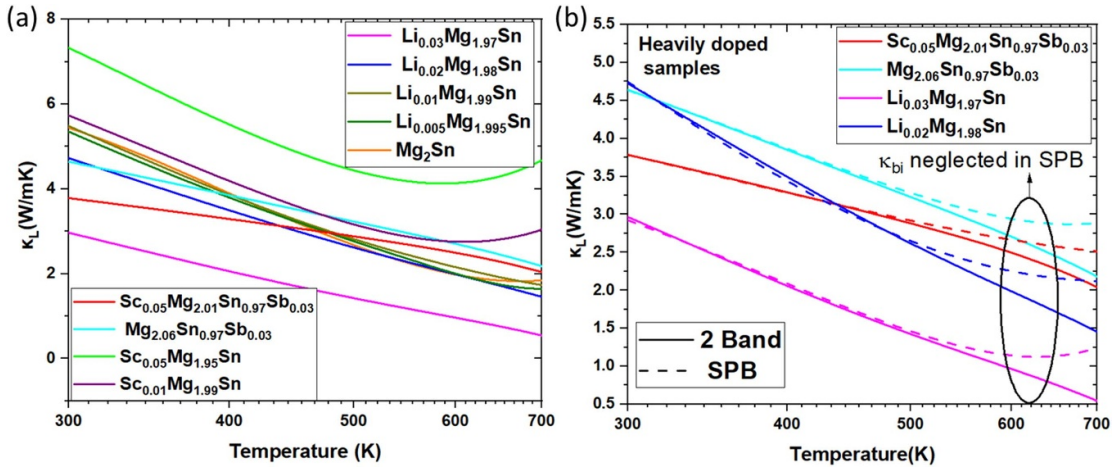

Figure 4. (a) Lattice thermal conductivity vs. temperature for all samples calculated from the two-band model (b) comparison of κ_L obtained from SPB and 2PB models for heavily doped samples. The SPB model overestimates κ_L at higher temperatures because it does not account for bipolar thermal conductivity (κ_{bi}).

and $b = 0$. Since extrinsic carrier concentrations for low doped samples are obtained from fitting after all two-band parameters were determined, their values naturally changed when fitting was attempted with different band gap values. A comparison of fitting with different band gap values is shown in figure S2 in the supplementary info for the low doped samples. At this point it should be mentioned that if the two-band model employed does not give a good match with the experimental data, additional model features like mixed scattering, temperature dependence of the DOS mass etc can be made. Naturally, this would lead to more complexity. Also, since the method uses the SPB model to determine band parameters, it can only be used in cases where one effective CB and one effective VB are sufficient to describe the extrinsic behavior adequately. If there are more than one band of either kind, the SPB model will predict effective parameters which might be physically inaccurate [26–28]. Since, for Mg_2Sn systems two CBs have been obtained by DFT, it is possible that the assumption of one effective CB is physically inadequate. Furthermore, a minor dependence of m_{D,CB^*} on carrier concentration has been observed [71] in contrast to the rigid band structure assumed here. However, such low doped samples are not of practical interest for thermogenerator applications and the presented model predicts HD behavior with good accuracy.

An additional check for the validity of the model is provided by calculating the lattice thermal conductivity for all samples. Bipolar thermal conductivity increases with temperature and can contribute significantly to the total thermal conductivity. Its underestimation can cause an increase in the band-modelling-calculated lattice thermal conductivity with temperature. Figure 4(a) shows the variation of lattice thermal conductivities calculated from a 2PB model for all the studied samples as a function of temperature (semi-logarithmic plot). The relevance of two-band modelling is further exemplified when one compares the values obtained from 2PB and SPB models. Figure 4(b) shows SPB-calculated κ_L for the HD samples. Even for HD samples, where SPB modelling is supposed to be applicable, at high temperatures the calculated κ_L increases, indicating that bipolar effect is not negligible in these samples as well. Omitting the two outliers, $Sc_{0.05}Mg_{1.95}Sn$ and $Li_{0.03}Mg_{1.97}Sn$, κ_L values for all samples lie between 4.5 and 6 W mK^{-1} at 300 K, which is a relatively broad range. As the samples were prepared by similar synthesis approaches we think that the main reasons for this are sample-to-sample variations as well as a reduction of κ_L due to doping, as observed e.g. in [72–75]. The calculated κ_L for the low doped samples increase with temperature for $T > 600$ K also with the employed 2PB model, however, much less than if an SPB model had been employed. This is not expected physically and indicates an underestimation of the bipolar effect for these samples, possibly linked to the not fully correct assumption of a constant effective mass. Nevertheless, the trend of lattice thermal conductivity for most samples, particularly the HD samples which are of practical interest, is as expected, indicating success of the model.

The most relevant information for practical applications that is obtained from band modelling is the optimum carrier concentration. For this purpose, zT vs n plots are obtained. To obtain a theoretical zT vs n plot using a two-band model, the two band masses and mobility parameters, band gap and lattice thermal conductivity are needed. The first three parameters were readily available from band modelling but due to a large variation among values, a suitable κ_L had to be carefully selected. Values of κ_L for all samples except the two outliers—$Sc_{0.05}Mg_{1.95}Sn$ and $Li_{0.03}Mg_{1.97}Sn$, and $Sc_{0.01}Mg_{1.99}Sn$ (showing significant underestimation of bipolar conduction)—were averaged. Then a $1/T^x$ fitting [76] was done to the averaged κ_L to use in zT vs n

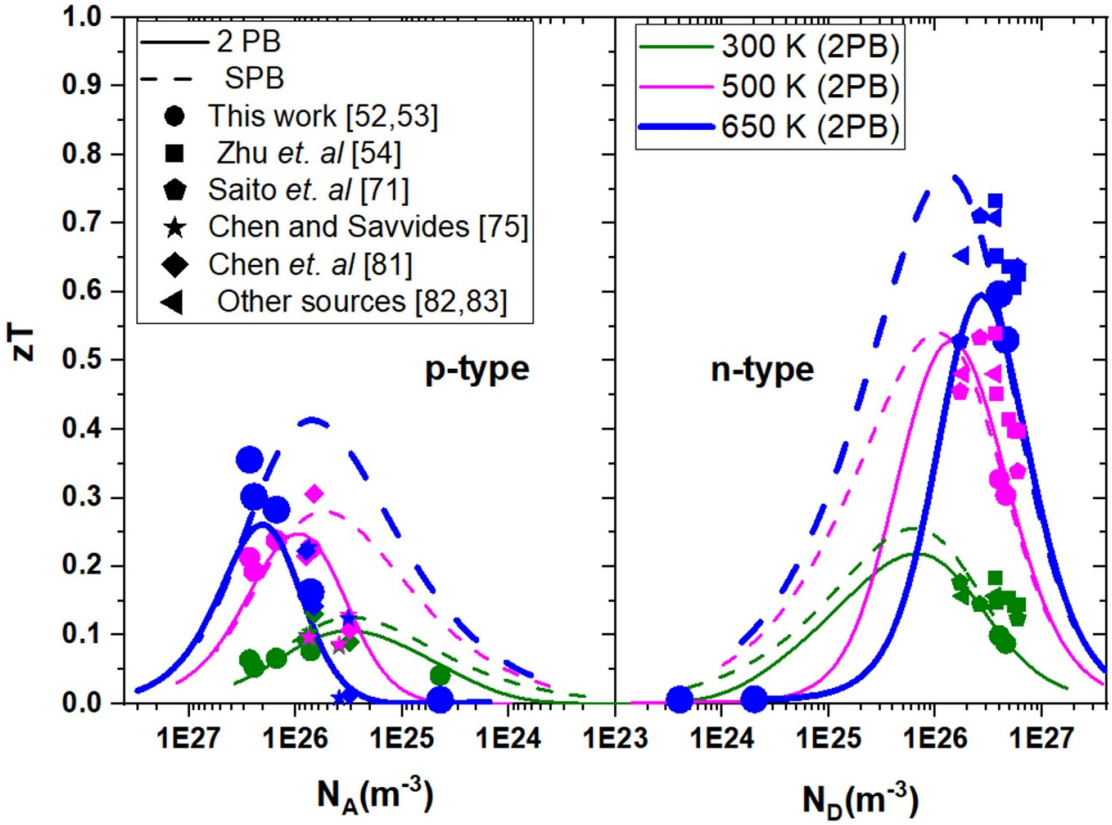

Figure 5. zT vs. $N_{extrinsic}$ (subscript A for net acceptor and D for net donor charge carriers). Comparison between SPB and 2PB is shown. Additional experimental data to test the general applicability of the model are taken from literature and the samples' details are given in table S2 of the supplementary info.

calculation. Similarly, κ_L is also required in the SPB-modelled zT vs n. With the intention of showing modelling result employing purely SPB analysis, κ_L obtained from SPB was used by averaging for three HD samples—$Li_{0.02}Mg_{1.98}Sn$, $Sc_{0.05}Mg_{2.01}Sn_{0.97}Sb_{0.03}$ and $Mg_{2.06}Sn_{0.97}Sb_{0.03}$. $Li_{0.03}Mg_{1.97}Sn$, though HD, was not used since its calculated lattice thermal conductivity was very different from the rest of the samples. $1/T^x$ fitting was again done to the averaged SPB κ_L. This fitting for SPB and two-band κ_L is shown in supplementary figure S3. Figure 5 shows zT vs $N_{extrinsic}$ plot for Mg_2Sn as obtained from SPB and the two-band model along with experimental data.

A few inferences can be readily made from figure 5. SPB clearly overestimates the maximum zT and underestimates the optimum carrier concentration. Also, SPB predicts a broader window of high zT than the 2PB model. Therefore, it becomes all the more important to predict the n_{opt} accurately within this narrow high zT window. Assuming that the 2PB model correctly predicts zT vs $N_{extrinsic}$, if the SPB-predicted n_{opt} were used to synthesize the sample, only 70% of the maximum possible zT would be attained. Note that for devices working across a temperature interval, zT is not optimized at a specific temperature. Rather, the averaged figure of merit is a better measure of efficiency [77]. Appropriate averages [78] as well as efficiency calculations considering the temperature dependence of the thermoelectric properties [79, 80] can be readily obtained using the model introduced here. Overall, the experimental data is captured well by the 2PB model. As expected, SPB does not capture the trends of low doped samples at all. For p-type samples, there is a good agreement with the 2PB model data except for $Li_{0.03}Mg_{1.97}Sn$ ($n_A = 2.7 \times 10^{26}$ m^{-3}). This is due to the low experimental lattice thermal conductivity of that sample which cannot be captured by the generalized two band model where an averaged κ_L has been employed. Among the n-type samples, the agreement with the modelled data is good for all temperatures and carrier concentrations. The model predicts an optimum extrinsic carrier concentration of 2.7×10^{26} m^{-3} for the n-type material and 2.0×10^{26} m^{-3} for the p-type material at 650 K. The zT_{max} for n-type is higher than that for p-type at all temperatures due to higher DOS mass of the CB (the mobility parameters are similar for both bands). Additional data were taken from literature [54, 71, 75, 81–83] to test the general applicability of the model parameters presented here. There is a decent agreement for most of the external data. For the data which shows disagreement it should be noted that the apparent better match with the SPB model is misleading: comparison at lower temperatures (where both models are similar) shows that the differences arise from different DOS masses and thermal

conductivities associated with the data. Some deviations from the model are expected due to different synthesis parameters which cannot be captured completely by a generalized band structure model.

5. Conclusion

A general method for implementing a two-band model has been presented here. The method uses the SPB equations to estimate DOS masses and mobility parameters for the valence and CBs from HD samples and then combines this information with two band equations to predict the band gap using data for all the samples for which extrinsic carrier concentrations can be determined. With the presented method, the band gap is quickly and reliably estimated as proven for Mg_2Sn. The knowledge of a material's band gap is crucial for modelling the effect of minority carriers and the key challenge in implementing a 2 PB model. While a good agreement between the modelled and experimental data was achieved for all Mg_2Sn samples for the electrical conductivity, the match for the Seebeck coefficient is not ideal for low doped samples which could be due to involvement of more than one band of majority carriers, dependence of the DOS mass on carrier concentration etc. Since low doped samples are usually not of practical interest for TE conversion, this can be considered a minor shortcoming of the model. An improved estimate for the lattice thermal conductivity can be obtained from a 2PB model compared to an SPB model even for HD samples. Apart from better modelling of TE properties, accurate estimation of lattice thermal conductivity is important if one is aiming to decrease lattice thermal conductivity—a popular strategy for increasing the figure of merit. Most importantly, a good match between experimental and modeled zT vs $N_{extrinsic}$ has been obtained. This is crucial since n_{opt} and zT_{max} are quantities of practical interest and in the prediction of these quantities lies the greatest utility of band structure modelling of TE transport properties. There is a decent agreement between the two-band model and the experimental data from different literature sources indicating some universality to the model. Owing to the generality and simplicity of the method presented here, 2PB modelling can be implemented on any typically band-conducting thermoelectric material system relatively easily. This will help in a more accurate determination of the optimum carrier concentration necessary for targeted material synthesis. A simple but accurate description of the TE transport can also set the foundation for integrated material-device simulations, guiding experimental efforts towards high device efficiency.

Data availability statement

All data that support the findings of this study are included within the article (and any supplementary files).

ORCID iDs

H Naithani https://orcid.org/0000-0001-9138-8431
J de Boor https://orcid.org/0000-0002-1868-3167

References

[1] Snyder G J and Toberer E S 2008 Complex thermoelectric materials *Nat. Mater.* **7** 105–14
[2] Sundarraj P, Maity D, Roy S S and Taylor R A 2014 Recent advances in thermoelectric materials and solar thermoelectric generators–a critical review *RSC Adv.* **4** 46860
[3] Zhao D and Tan G 2014 A review of thermoelectric cooling: materials, modeling and applications *Appl. Therm. Eng.* **66** 15
[4] Orr B, Akbarzadeh A, Mochizuki M and Singh R 2016 A review of car waste heat recovery systems utilising thermoelectric generators and heat pipes *Appl. Therm. Eng.* **101** 490
[5] Champier D 2017 Thermoelectric generators: a review of applications *Energy Convers. Manage.* **140** 167
[6] Tan G, Zhao L-D and Kanatzidis M G 2016 Rationally designing high-performance bulk thermoelectric materials *Chem. Rev.* **116** 12123
[7] Hao Q, Xu D, Lu N and Zhao H 2016 High-throughput Z T predictions of nanoporous bulk materials as next-generation thermoelectric materials: a material genome approach *Phys. Rev.* B **93** 205206
[8] Sherchenkov A, Shtern Y I, Mironov R, Shtern M Y and Rogachev M 2015 Current state of thermoelectric material science and the search for new effective materials *Nanotechnol. Russ.* **10** 827
[9] Pei Y, Wang H and Snyder G J 2012 Band engineering of thermoelectric materials *Adv. Mater.* **24** 6125
[10] He J and Tritt T M 2017 Advances in thermoelectric materials research: looking back and moving forward *Science* **357** eaak9997
[11] Hu L, Zhu T, Liu X and Zhao X 2014 Point defect engineering of high-performance bismuth-telluride-based thermoelectric materials *Adv. Funct. Mater.* **24** 5211
[12] Li Z, Xiao C, Zhu H and Xie Y 2016 Defect chemistry for thermoelectric materials *J. Am. Chem. Soc.* **138** 14810
[13] Mao J, Wu Y, Song S, Zhu Q, Shuai J, Liu Z, Pei Y and Ren Z 2017 Defect engineering for realizing high thermoelectric performance in n-type Mg_3Sb_2-based materials *ACS Energy Lett.* **2** 2245
[14] Zheng Y, Slade T J, Hu L, Tan X Y, Luo Y, Luo Z-Z, Xu J, Yan Q and Kanatzidis M G 2021 Defect engineering in thermoelectric materials: what have we learned? *Chem. Soc. Rev.* **50** 9022–54
[15] Pei Y, LaLonde A D, Heinz N A, Shi X, Iwanaga S, Wang H, Chen L and Snyder G J 2011 Stabilizing the optimal carrier concentration for high thermoelectric efficiency *Adv. Mater.* **23** 5674

[16] May A F and Snyder G J 2012 Introduction to modeling thermoelectric transport at high temperatures *Materials, Preparation, Characterization in Thermoelectrics* vol **1** (Boca Raton, FL: CRC Press) p 18
[17] Böttger P M, Pomrehn G S, Snyder G J and Finstad T G 2011 Doping of p-type ZnSb: single parabolic band model and impurity band conduction *Phys. Status Solidia* **208** 2753
[18] Shen J, Chen Z, Zheng L, Li W and Pei Y 2016 Single parabolic band behavior of thermoelectric p-type $CuGaTe_2$ *J. Mater. Chem.* C **4** 209
[19] Wang X, Li W, Wang C, Li J, Zhang X, Zhou B, Chen Y and Pei Y 2017 Single parabolic band transport in p-type $EuZn_2Sb_2$ thermoelectrics *J. Mater. Chem.* A **5** 24185
[20] Toberer E S, Rauwel P, Gariel S, Taftø J and Snyder G J 2010 Composition and the thermoelectric performance of β-Zn_4Sb_3 *J. Mater. Chem.* **20** 9877
[21] Li W, Zhou B, Li J, Zhu S and Li J 2018 Single parabolic band behavior of thermoelectric p-type $Cu_4Mn_2Te_4$ *J. Alloys Compd.* **753** 93
[22] Liu W, Chi H, Sun H, Zhang Q, Yin K, Tang X, Zhang Q and Uher C 2014 Advanced thermoelectrics governed by a single parabolic band: $Mg_2Si_{0.3}Sn_{0.7}$, a canonical example *Phys. Chem. Chem. Phys.* **16** 6893
[23] Wang S, Li H, Lu R, Zheng G and Tang X 2013 Metal nanoparticle decorated n-type Bi_2Te_3-based materials with enhanced thermoelectric performances *Nanotechnology* **24** 285702
[24] Pei Y, May A F and Snyder G J 2011 Self-tuning the carrier concentration of PbTe/Ag_2Te composites with excess Ag for high thermoelectric performance *Adv. Energy Mater.* **1** 291
[25] Zhang Q, Wang H, Zhang Q, Liu W, Yu B, Wang H, Wang D, Ni G, Chen G and Ren Z 2012 Effect of silicon and sodium on thermoelectric properties of thallium-doped lead telluride-based materials *Nano Lett.* **12** 2324
[26] Naithani H and Dasgupta T 2019 Critical analysis of single band modeling of thermoelectric materials *ACS Appl. Energy Mater.* **3** 2200
[27] de Boor J 2021 On the applicability of the single parabolic band model to advanced thermoelectric materials with complex band structures *J. Materiomics* **7** 603
[28] Wang H, Gurunathan R, Fu C, Cui R, Zhu T and Snyder G J 2022 Thermoelectric transport effects beyond single parabolic band and acoustic phonon scattering *Mater. Adv.* **3** 734
[29] O'donnell K and Chen X 1991 Temperature dependence of semiconductor band gaps *Appl. Phys. Lett.* **58** 2924
[30] Varshni Y P 1967 Temperature dependence of the energy gap in semiconductors *Physica* **34** 149
[31] Chasapis T C, Koumoulis D, Leung B, Calta N P, Lo S H, Dravid V P, Bouchard L S and Kanatzidis M G 2015 Two-band model interpretation of the p- to n-transition in ternary tetradymite topological insulators *APL Mater.* **3** 083601
[32] de Boor J, Berche A and Jund P 2020 Density of states effective mass for p-type Mg_2Si–Mg_2Sn solid solutions: comparison between experiments and first-principles calculations *J. Phys. Chem.* C **124** 14987
[33] Kutorasinski K, Wiendlocha B, Tobola J and Kaprzyk S 2014 Importance of relativistic effects in electronic structure and thermopower calculations for Mg_2Si, Mg_2Ge, and Mg_2Sn *Phys. Rev.* B **89** 115205
[34] Burke K 2012 Perspective on density functional theory *J. Chem. Phys.* **136** 150901
[35] Morales-García Á, Valero R and Illas F 2017 An empirical, yet practical way to predict the band gap in solids by using density functional band structure calculations *J. Phys. Chem.* C **121** 18862
[36] Crowley J M, Tahir-Kheli J and Goddard W A III 2016 Resolution of the band gap prediction problem for materials design *J. Phys. Chem. Lett.* **7** 1198
[37] Farahi N *et al* 2019 Effects of Ta substitution on the microstructure and transport properties of Hf-doped NbFeSb half-Heusler thermoelectric materials *ACS Appl. Energy Mater.* **2** 8244
[38] Kutorasiński K, Tobola J and Kaprzyk S 2013 Calculating electron transport coefficients of disordered alloys using the KKR-CPA method and Boltzmann approach: application to $Mg_2Si_{1-x}Sn_x$ thermoelectrics *Phys. Rev.* B **87** 195205
[39] Akasaka M, Iida T, Matsumoto A, Yamanaka K, Takanashi Y, Imai T and Hamada N 2008 The thermoelectric properties of bulk crystalline n- and p-type Mg_2Si prepared by the vertical Bridgman method *J. Appl. Phys.* **104** 013703
[40] Kim S, Wiendlocha B, Jin H, Tobola J and Heremans J P 2014 Electronic structure and thermoelectric properties of p-type Ag-doped Mg_2Sn and $Mg_2Sn_{1-x}Si_x$ ($x = 0.05, 0.1$) *J. Appl. Phys.* **116** 153706
[41] Liu W *et al* 2015 n-type thermoelectric material $Mg_2Sn_{0.75}Ge_{0.25}$ for high power generation *Proc. Natl Acad. Sci.* **112** 3269
[42] Zaitsev V, Fedorov M, Gurieva E, Eremin I, Konstantinov P, Samunin A Y and Vedernikov M 2006 Highly effective $Mg_2Si_{1-x}Sn_x$ thermoelectrics *Phys. Rev.* B **74** 045207
[43] Zhang L, Xiao P, Shi L, Henkelman G, Goodenough J B and Zhou J 2015 Suppressing the bipolar contribution to the thermoelectric properties of $Mg_2Si_{0.4}Sn_{0.6}$ by Ge substitution *J. Appl. Phys.* **117** 155103
[44] Yasseri M, Mitra K, Sankhla A, de Boor J and Müller E 2021 Influence of Mg loss on the phase stability in Mg_2X (X = Si, Sn) and its correlation with coherency strain *Acta Mater.* **208** 116737
[45] Yasseri M, Sankhla A, Kamila H, Orenstein R, Truong D Y N, Farahi N, de Boor J and Mueller E 2020 Solid solution formation in Mg_2(Si,Sn) and shape of the miscibility gap *Acta Mater.* **185** 80
[46] Orenstein R, Male J P, Toriyama M, Anand S and Snyder G J 2021 Using phase boundary mapping to resolve discrepancies in the Mg_2Si–Mg_2Sn miscibility gap *J. Mater. Chem.* A **9** 7208
[47] Jung I H, Kang D H, Park W J, Kim N J and Ahn S 2007 Thermodynamic modeling of the Mg–Si–Sn system *Calphad* **31** 192
[48] Ryu B, Park S, Choi E-A, de Boor J, Ziolkowski P, Chung J and Park S D 2019 Hybrid-functional and quasi-particle calculations of band structures of Mg_2Si, Mg_2Ge, and Mg_2Sn *J. Korean Phys. Soc.* **75** 144
[49] Winkler U E 1955 Die elektrischen Eigenschaften der intermetallischen Verbindungen Mg_2Si, Mg_2Ge, Mg_2Sn und Mg_2Pb *Doctoral Thesis* ETH Zurich
[50] Bahk J-H, Bian Z and Shakouri A 2014 Electron transport modeling and energy filtering for efficient thermoelectric $Mg_2Si_{1-x}Sn_x$ solid solutions *Phys. Rev.* B **89** 075204
[51] Shi G and Kioupakis E 2018 Relativistic quasiparticle band structures of Mg_2Si, Mg_2Ge, and Mg_2Sn: consistent parameterization and prediction of Seebeck coefficients *J. Appl. Phys.* **123** 085114
[52] Sankhla A, Yasseri M, Kamila H, Mueller E and de Boor J 2019 Experimental investigation of the predicted band structure modification of Mg_2 X (X: Si, Sn) thermoelectric materials due to scandium addition *J. Appl. Phys.* **125** 225103
[53] Kamila H, Sahu P, Sankhla A, Yasseri M, Pham H-N, Dasgupta T, Mueller E and de Boor J 2019 Analyzing transport properties of p-type Mg_2 Si–Mg_2Sn solid solutions: optimization of thermoelectric performance and insight into the electronic band structure *J. Mater. Chem.* A **7** 1045
[54] Zhu Y, Han Z, Jiang F, Dong E, Zhang B-P, Zhang W and Liu W 2021 Thermodynamic criterions of the thermoelectric performance enhancement in Mg_2Sn through the self-compensation vacancy *Mater. Today Phys.* **16** 100327

[55] Vining C B 1991 A model for the high-temperature transport properties of heavily doped n-type silicon-germanium alloys *J. Appl. Phys.* **69** 331
[56] Herring C and Vogt E 1957 Transport and deformation-potential theory for many-valley semiconductors with anisotropic scattering *Phys. Rev.* **105** 1933
[57] Harrison J W and Hauser J R 1976 Alloy scattering in ternary III–V compounds *Phys. Rev.* B **13** 5347
[58] Liu X, Zhu T, Wang H, Hu L, Xie H, Jiang G, Snyder G J and Zhao X 2013 Low electron scattering potentials in high performance $Mg_2Si_{0.45}Sn_{0.55}$ based thermoelectric solid solutions with band convergencec *Adv. Energy Mater.* **3** 1238
[59] Callaway J 1959 Model for lattice thermal conductivity at low temperatures *Phys. Rev.* **113** 1046
[60] de Boor J, Dasgupta T, Kolb H, Compere C, Kelm K and Müller E 2014 Microstructural effects on thermoelectric efficiency: a case study on magnesium silicide *Acta Mater.* **77** 68
[61] Sankhla A, Kamila H, Kelm K, Mueller E and de Boor J 2020 Analyzing thermoelectric transport in n-type $Mg_2Si_{0.4}Sn_{0.6}$ and correlation with microstructural effects: an insight on the role of Mg *Acta Mater.* **199** 85
[62] Kato D and Iwasaki K 2021 Mg-pressure-controlled annealing for tuning Mg content and thermoelectric properties of $Mg_{2-\delta}(Si0.5Sn0.5)_{1-x}Sb_x$ *J. Alloys Compd.* **856** 157351
[63] Wood M, Kuo J J, Imasato K and Snyder G J 2019 Improvement of low-temperature zT in a Mg_3Sb_2–Mg_3Bi_2 solid solution via Mg-vapor annealing *Adv. Mater.* **31** 1902337
[64] Kuo J J, Kang S D, Imasato K, Tamaki H, Ohno S, Kanno T and Snyder G J 2018 Grain boundary dominated charge transport in Mg_3Sb_2-based compounds *Energy Environ. Sci.* **11** 429
[65] Seto J Y 1975 The electrical properties of polycrystalline silicon films *J. Appl. Phys.* **46** 5247
[66] Goldsmid H J and Sharp J W 1999 Estimation of the thermal band gap of a semiconductor from seebeck measurements *J. Electron. Mater.* **28** 869
[67] Gibbs Z M, Kim H-S, Wang H and Snyder G J 2015 Band gap estimation from temperature dependent Seebeck measurement—deviations from the $2e|S|_{max}T_{max}$ relation *Appl. Phys. Lett.* **106** 022112
[68] Blunt R F, Frederikse H P R and Hosler W R 1955 Electrical and optical properties of intermetallic compounds. IV. Magnesium stannide *Phys. Rev.* **100** 663
[69] Norouzzadeh P and Vashaee D 2015 The effect of multivalley bandstructure on thermoelectric properties of $Al_xGa_{1-x}As$ *J. Electron. Mater.* **44** 636
[70] Tang Y, Gibbs Z M, Agapito L A, Li G, Kim H-S, Nardelli M B, Curtarolo S and Snyder G J 2015 Convergence of multi-valley bands as the electronic origin of high thermoelectric performance in $CoSb_3$ skutterudites *Nat. Mater.* **14** 1223
[71] Saito W, Hayashi K, Huang Z, Dong J, Li J-F and Miyazaki Y 2020 Enhancing the thermoelectric performance of Mg_2Sn single crystals via point defect engineering and Sb doping *ACS Appl. Mater. Interfaces* **12** 57888
[72] de Boor J, Dasgupta T, Saparamadu U, Müller E and Ren Z F 2017 Recent progress in p-type thermoelectric magnesium silicide based solid solutions *Mater. Today Energy* **4** 105
[73] Nieroda P, Kolezynski A, Oszajca M, Milczarek J and Wojciechowski K T 2016 Structural and thermoelectric properties of polycrystalline p-type $Mg_{2-x}Li_xSi$ *J. Electron. Mater.* **45** 3418
[74] Tani J-I and Kido H 2005 Thermoelectric properties of Bi-doped Mg_2Si semiconductors *Physica* B **364** 218
[75] Chen H and Savvides N 2010 High quality Mg_2Sn crystals prepared by RF induction melting *J. Cryst. Growth* **312** 2328
[76] Tritt T M 2005 *Thermal Conductivity: Theory, Properties, and Applications* (New York: Springer)
[77] Armstrong H, Boese M, Carmichael C, Dimich H, Seay D, Sheppard N and Beekman M 2017 Estimating energy conversion efficiency of thermoelectric materials: constant property versus average property models *J. Electron. Mater.* **46** 6
[78] Ponnusamy P, de Boor J and Müller E 2020 Using the constant properties model for accurate performance estimation of thermoelectric generator elements *Appl. Energy* **262** 114587
[79] Ponnusamy P, Kamila H, Müller E and de Boor J 2021 Efficiency as a performance metric for material optimization in thermoelectric generators *J. Phys. Energy* **3** 044006
[80] Kim H S, Liu W and Ren Z J E 2017 The bridge between the materials and devices of thermoelectric power generators *Energy Environ. Sci.* **10** 69
[81] Chen H, Savvides N, Dasgupta T, Stiewe C and Mueller E 2010 Electronic and thermal transport properties of Mg_2Sn crystals containing finely dispersed eutectic structures *Phys. Status Solidi* a **207** 2523
[82] Liu W, Zhou J, Jie Q, Li Y, Kim H S, Bao J, Chen G and Ren Z 2016 New insight into the material parameter B to understand the enhanced thermoelectric performance of $Mg_2Sn_{1-x-y}Ge_xSb_y$ *Energy Environ. Sci.* **9** 530
[83] Mao J, Wang Y, Ge B, Jie Q, Liu Z, Saparamadu U, Liu W and Ren Z 2016 Thermoelectric performance enhancement of Mg_2Sn based solid solutions by band convergence and phonon scattering via Pb and Si/Ge substitution for Sn *Phys. Chem. Chem. Phys.* **18** 20726